Instabilities in magnetized spherical Couette flow

Christophe Gissinger,[1,2] Hantao Ji,[2] and Jeremy Goodman[1]

[1] *Department of Astrophysical Sciences, Princeton University, Princeton, NJ 08544.*
[2] *Center for Magnetic Self-Organization in Laboratory and Astrophysical Plasmas, Princeton Plasma Physics Laboratory, Princeton University, P.O. Box 451, Princeton, New Jersey 08543, USA*

We report 3D numerical simulations of the flow of an electrically conducting fluid in a spherical shell when an magnetic field is applied. Different spherical Couette configurations are investigated, by varying the rotation ratio between the inner and the outer sphere, the geometry of the imposed field, and the magnetic boundary conditions on the inner sphere. Either a Stewartson layer or a Shercliff layer, accompanied by a radial jet, can be generated depending on the rotation speeds and the magnetic field strength, and various non-axisymmetric destabilizations of the flow are observed. We show that instabilities arising from the presence of boundaries present striking similarities with the magnetorotational instability (MRI). To this end, we compare our numerical results to experimental observations of the Maryland experiment, who claimed to observe MRI in a similar setup.

PACS numbers: 47.65.-d, 52.65.Kj, 91.25.Cw

arXiv:1106.0319v1 [physics.flu-dyn] 1 Jun 2011

INTRODUCTION

Spherical Couette flow, i.e. the flow between differentially rotating concentric spheres, has attracted a revival of interest in recent years. It has been shown that despite the simplicity of the problem, the flow undergoes many bifurcations as Reynolds number increases, depending in ratios of sphere radii and rotation speeds. When one considers an electrically conducting fluid and imposes magnetic field, magnetohydrodynamic effects can significantly change the purely hydrodynamical problem and lead to new instabilities. This problem has evident consequences in geophysical and astrophysical contexts (stars, planetary interiors), where setups similar to magnetized spherical Couette flow are often encountered.

This problem has also been extensively studied in cylindrical Taylor-Couette flow, i.e. the viscous flow between two differentially rotating concentric cylinders. This interest in magnetized conducting fluids confined by rotating walls has been renewed in the last decade by investigation of the magnetorotational instability (MRI) in the laboratory. The MRI is currently the best candidate to explain angular momentum transport in accretion disks around stars and black holes [1]. Balbus and Hawley, rediscovering an instability first studied by Velikhov[2] and Chandrasekhar [4], have shown that a weak magnetic field can destabilize otherwise stable Keplerian flows. The MRI eventually yields a magnetohydrodynamical turbulent state, enhancing the angular momentum transport and allowing inward flow, as observed in accretion disks.

Several experiments are currently working on this instability. The Princeton experiment has been designed to observe MRI in a Taylor-Couette flow of liquid Gallium, with an axial applied magnetic field [5]. So far, MRI has not been identified, but non-axisymmetric modes have been observed when a strong magnetic field is imposed [6]. The PROMISE experiment, in Dresden, is based on a similar set-up, except that the applied field possesses an azimuthal component. Axisymmetric traveling waves have been obtained, and identified as being Helical MRI, an inductionless instability different from but connected to the standard MRI [7].

On the other hand, spherical Couette flows have been widely studied, through theoretical analyses, laboratory experiments, and numerical simulations. For instance, without magnetic field but for sufficiently large Reynolds numbers, it is known that the flow can be hydrodynamically unstable to a rich variety of axisymmetric and non-axisymmetric modes. When a magnetic field is applied, additional magnetohydrodynamic effects are generated. Hollerbach [9] first shows numerically that a free shear layer is created in the flow when a strong magnetic field is imposed. This configuration was later asymptotically analyzed by Kleeorin et al [10] and Starchenko [11]. When the inner sphere is conducting, Dormy et al [12] discovered that imposing a dipolar magnetic field yields a super-rotating jet, that is, a region of fluid with angular velocity larger than either boundary's. This super-rotation was recently observed experimentally in the DTS experiment, using a spherical shell filled with liquid Sodium in presence of a dipolar magnetic field imposed by a permanent magnet inside the inner sphere [13],[14]. More recently, it was shown that several non-axisymmetric instabilities are generated from these magnetized spherical Couette flows, including destabilization of the meridional return flow [15],[16], or from the free shear layers and jets produced by the magnetic field [17], [18].

A few years ago, it has been claimed that MRI was obtained in a spherical Couette flow of liquid Sodium in Maryland [8]. In this experiment, in which the outer sphere is at rest and an external axial magnetic field is applied parallel to the rotation axis, non-axisymmetric

oscillations of both velocity and magnetic fields have been observed, together with an increase of the torque on the inner sphere. Although the instability appears from a hydrodynamical state already turbulent, these oscillations have been interpreted as a signature of the MRI.

In this article, we numerically investigate magnetized spherical Couette flow for different configurations, including a setup similar to the Maryland experiment. In the first section, we present the equations and the numerical method used to study this problem. In sections II and III, we report numerical simulations with a dipolar magnetic field applied to the flow, and with a rotating outer sphere. We show that magnetized spherical Couette flow yield different non-axisymmetric instabilities with a rich variety of structures and non-linear interactions. We compare our MHD instabilities to the MRI, and highlight the striking similarities between both type of instabilities, including the enhancement of angular momentum transport and the transition to MHD turbulence. Finally, our numerical results using an axial magnetic field are directly compared to the Maryland experiment.

I EQUATIONS

We consider the flow of an electrically conducting fluid induced in a spherical shell. The aspect ratio of the inner sphere radius r_i to the outer radius r_o is set to 0.35. Ω_i and Ω_o are respectively the angular speed of the inner and the outer sphere. The governing equations for this problem are the Navier-Stokes equations coupled to the induction equation :

$$\rho\frac{\partial \mathbf{u}}{\partial t} + \rho\left(\mathbf{u}\nabla\right)\mathbf{u} = -\nabla P + \rho\nu\nabla^2\mathbf{u} + \mathbf{j}\times\mathbf{B}\ . \qquad (1)$$

$$\frac{\partial \mathbf{B}}{\partial t} = \nabla\times\left(\mathbf{u}\times\mathbf{B}\right) + \frac{1}{\mu_0\sigma}\nabla^2\mathbf{B}\ . \qquad (2)$$

where ρ is the density, ν the kinematic viscosity, $\eta = 1/(\sigma\mu_0)$ is the electrical resistivity, $\mathbf{u}$ is the fluid velocity and $\mathbf{B}$ the magnetic field. Lengths are scaled by the shell gap $l_0 = r_o - r_i$, and we use the viscous time $t_0 = l_0^2/\nu$ as a typical time scale. The magnetic field $\mathbf{B}$ is scaled by $\sqrt{\rho\mu_0\eta\Omega_i}$. The problem is thus characterized by 3 dimensionless numbers: the Reynolds number $Re = (\Omega_i l_0^2)/\nu$, the magnetic Reynolds number $Rm = (\Omega_i l_0^2)/\eta$ and the Elsasser number $\Lambda = B_0/\sqrt{\Omega_i\rho\mu_0\eta}$. It is also useful to define the magnetic Prandtl number $Pm = \nu/\eta$, which is simply the ratio between Reynolds numbers. The magnetic and kinetic energies reported in this article are respectively scaled by $\rho\nu\Omega_i$ and $\rho\nu^2/l_0^2$, and the torques by $\rho\nu l_0$. These equations are numerically integrated using the PARODY code [12],[19]. In this code, velocity and magnetic fields are decomposed in poloidal and toroidal components and expanded in spherical harmonics. In the radial direction, a finite differences method is used on an irregular mesh, which decreases in geometrical progression towards the boundaries. Time stepping is implemented by a Crank-Nicholson scheme for the diffusive terms and an Adams-Bashforth for the non-linear terms. Depending on the values of our dimensionless numbers, typical numerical resolutions involve between 150 and 250 radial grid points and between 64 and 150 spherical harmonics degrees and orders.

Magnetized spherical Couette flow has been largely studied in an interesting series of papers [17], [15], [18] and some of these results are confirmed by the present work. However, these previous studies rely on the assumption that the magnetic Reynolds number Rm can be neglected for very resistive fluids. This assumption greatly simplifies the governing equations, in particular the time derivative can be omitted from the induction equation (2). This is one of the motivations for the present study, since induction processes could play an important role when describing liquid metal experiments. In particular, a finite value of Rm is necessary to observe the standard magnetorotational instability. For instance, in the Maryland experiment (initially designed to observe dynamo action), the electrical conductivity of the liquid Sodium yields magnetic Reynolds numbers up to 30, meaning that Rm can no longer be neglected in the MHD equations.

II DIPOLAR MAGNETIC FIELD AND GLOBAL ROTATION

In this section and the next one, the inner sphere is rotating such that $\Omega_i/\Omega_o = 8$. The global rotation of the system is thus relatively weak. This configuration is particularly interesting in the context of MRI experiments. Indeed, in a cylindrical geometry, this choice of the rotation ratio would correspond to a system slightly below the Rayleigh stability criterion, but MRI unstable. Both spheres are taken insulating and an internal dipolar magnetic field (held by the inner sphere) is applied to the system. The magnetic Prandtl number is set to 1 in this section.

For small Reynolds numbers and with no magnetic field applied, the solution is axisymmetric and corresponds to the well known spherical Couette solution. It consists of a strong azimuthal flow associated with a poloidal recirculation. The Taylor-Proudman theorem states that for a sufficiently strong global rotation of the system, the velocity tends to be uniform in the z direction, due to a dominant balance between the pressure gradient and the Coriolis force [20]. As a consequence, the flow outside the tangent cylinder is in solid body rotation with the outer sphere. The difference of rotation between inner and outer spheres, together with the

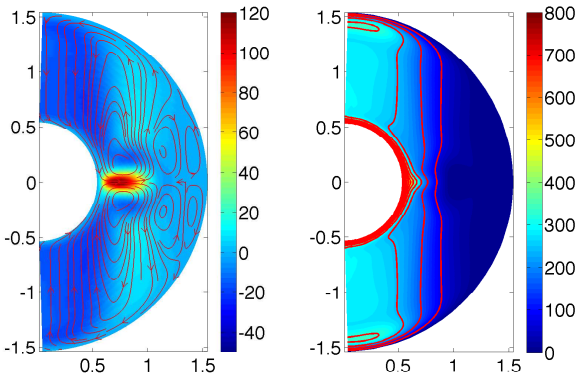


FIG. 1: Purely hydrodynamical Couette flow, obtained for $Re = 2000$ and $\Omega_i/\Omega_o = 8$. Left: Radial component u_r of the axisymmetric velocity. Note the strong equatorial jet in the midplane. (lines represent streamlines of the axisymmetric poloidal recirculation). Right: angular velocity in the meridional plane, showing a broad Stewartson layer on the tangent cylinder. Contours of Ω are also shown.

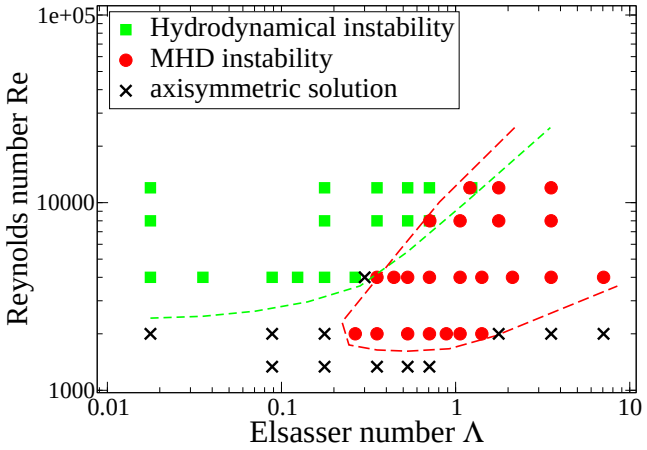


FIG. 2: Parameter space for a dipolar magnetic field applied to a system such that $\Omega_i = 8\Omega_o$, and with insulating spheres. Green squares indicate $m = 2$ hydrodynamical instabilities modified (and suppressed at large Λ) by the applied field. Red circles are MHD instabilities of the return flow or the free shear layer triggered by the magnetic field, dominated by $m = 1$ and $m = 2$ azimuthal wavenumbers. Black crosses indicate classical spherical Couette solutions, purely axisymetric.

Taylor-Proudman constraint, yield the so-called Stewartson free shear layer, located on the tangent cylinder [21]. Inside the Stewartson layer, the azimuthal flow rapidly varies from the velocity of the outer sphere (outside the tangent cylinder) to a velocity intermediate between inner and outer spheres (inside the tangent cylinder). The structure of the axisymmetric component of the flow for $Re = 2000$ is illustrated in figure 1, and shows a Stewartson layer developing on the tangent cylinder. Note that since these numerical simulations involve a relatively weak global rotation, the Stewartson layer is diffuse. Moreover, because of the differential rotation between the inner and the outer sphere, the poloidal recirculation is characterized by a strong equatorial jet in the midplane. A similar jet can be observed in Taylor-Couette flow with short aspect ratio (see for instance [22]).

For sufficiently large Reynolds number, this axisymmetric state becomes unstable to non-axisymmetric perturbations. Figure 2 shows the different states obtained in the parameter space (Re, Λ), and their corresponding marginal stability curves. For $Re > 2000$, the destabilization of the spherical Couette flow yields a non-axisymmetric instability, strongly dominated by the azimuthal wavenumber $m = 2$ (green squares in figure 2).

In figure 3 (bottom), we report the structure of this hydrodynamical instability by showing the non-axisymmetric radial component of the velocity field. The non-axisymmetric pattern drifts at a constant speed in the azimuthal direction. A cut in the equatorial plane (left) shows the $m = 2$ structure of the instability, and the meridional plane (right) illustrates its symmetry with respect to the equatorial plane. Following [15], we denote this state by 'symmetric', i.e. velocity and magnetic fields satisfy:

$$(u_r, u_\theta, u_\phi, B_r, B_\theta, B_\phi)\,(r, \theta, \phi) = (u_r, -u_\theta, u_\phi, -B_r, B_\theta, -B_\phi)\,(r, \pi - \theta, \phi) \quad (3)$$

whereas antisymmetric modes satisfy:

$$(u_r, u_\theta, u_\phi, B_r, B_\theta, B_\phi)\,(r, \theta, \phi) = (-u_r, u_\theta, -u_\phi, B_r, -B_\theta, B_\phi)\,(r, \pi - \theta, \phi) \quad (4)$$

In such spherical Couette flows, two distinct situations are generally considered: configurations with a strong global rotation, or configurations with the outer sphere at rest. Two types of instability are thus observed when Re is increased: In the first case, the Stewartson layer is destabilized and rolls up into a series of vortices in the (r, ϕ) plane, leading to an equatorially symmetric mode localized on the tangent cylinder. In the second case, if Re is sufficiently large, the strong equatorial jet becomes unstable by adopting a wavy structure, and yields an antisymmetric mode localized in the equatorial plane. In the present configuration, global rotation is relatively small and Reynolds numbers are large enough for both instabilities to be generated, so the interpretation is not as clear-cut. Indeed, as it can be seen in figure 3, the instability is symmetric with respect to the equator and

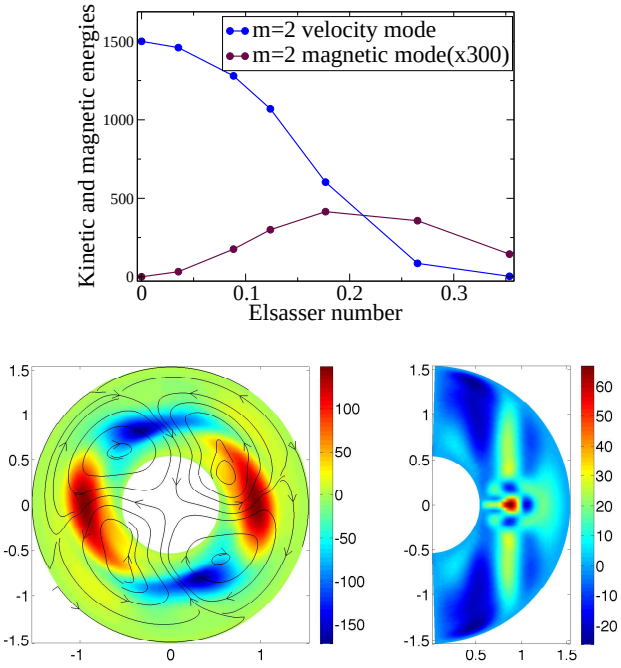


FIG. 3: Top: Evolution of magnetic and velocity modes when the Elsasser number is increased, for $Re = 4000$. The hydrodynamical $m = 2$ non-axisymmetric instability is suppressed by the action of the applied dipolar magnetic field. Bottom: Non-axisymmetric u_r showing the structure of the hydrodynamical instability in the equatorial plane (left) and in a meridional plane at $\phi = 0$ (right), for $Re = 4000$ and $\Lambda = 0$. On the left are also indicated streamlines of the horizontal flow of the instability integrated in the z-direction.

consists of a series of vortices in the horizontal plane (i.e. the velocity perturbations are mainly horizontal), as it is expected from a Stewartson layer instability. Note however that a large part of the energy of the mode is localized in the equatorial plane, suggesting the the system is close to a transition to an equatorial jet instability.

When a magnetic field is applied to this new hydrodynamical state, the instability can be suppressed: the flow is hydrodynamically unstable only in a limited pocket in the parameter space (suggested by the green dashed line in figure 2). Figure 3 (top) shows a bifurcation diagram of the $m = 2$ component of the kinetic and magnetic energies when Λ is increased, for $Re = 4000$. It illustrates the inhibiting role of the magnetic field: this $m = 2$ non-axisymmetric mode is strongly damped by the applied field. It is interesting to note that the observation of the magnetic energy alone would rather suggests a destabilizing effect of the magnetic field. For $\Lambda \sim 0.35$, the instability is completely suppressed, and the solution is back to an axisymmetric state.

In addition to this stabilizing effect, the applied magnetic field is also able to drive instabilities. In figure 2, the red circle indicate non-axisymmetric states, different from the hydrodynamical instabilities described previously.

This has been interpreted as a destabilization of the poloidal return flow by the applied field. In recent inductionless simulations, Hollerbach [15] has shown that in the presence of a weak magnetic field, the poloidal return flow is destabilized to a non-axisymmetric state. As the intensity of the magnetic field is increased, this instability continuously connects to another type of instability related to a free shear layer in the flow. Indeed, when a strong magnetic field is applied to a spherical Couette flow, the magnetic tension couples fluid elements together along the direction of magnetic field lines. This creates a particular surface Σ in the flow, separating the region where magnetic field lines are connected to both spheres from the region where magnetic field lines are only touching one of the sphere. Depending on the region considered, the flow will behave very differently. For instance, when the applied field is dipolar, like in this section, Σ is defined by magnetic field lines just touching the outer sphere at the equator. In this case, the fluid inside Σ, coupled only to the inner sphere, co-rotates with it, whereas fluid outside Σ rotates at an intermediate velocity (except near the sphere boundaries). The jump of velocity on the surface Σ therefore results in a new free layer, the so-called Shercliff layer [23]. This effect was first described in spherical geometry by Starchenko [11], who found that the thickness of this layer scales like $(\Lambda\sqrt{Re})^{-1/2}$. Like the Stewartson layer, the Shercliff layer becomes unstable to non-axisymmetric perturbations when the shear is strong enough. However, in the case of a dipolar applied field, the significance of the field lines Σ can be completely eliminated if the Reynolds number is large enough [24], and only instabilities of the return flow will remain. Despite the differences in the geometry of the applied field and in the parameter regime, it is surprising to note that our figure 2 is very similar to Fig.2 of [15].

Figure 4 shows the evolution of the non-axisymmetric components of the magnetic field when the Elsasser number is increased, for $Re = 2000$. For this small Reynolds number, both Stewartson layer and equatorial jet are hydrodynamically stable to non-axisymmetric perturbations for $\Lambda = 0$. As Λ is increased from this axisymmetric state, the return flow becomes unstable, and the system undergoes a bifurcation to an $m = 1$ rotating mode at $\Lambda_c = 0.2$ (corresponding to red dots in figure 2).

When Λ is increased further, one observes a transfer between this $m = 1$ mode and an $m = 2$ structure. Figure 5 shows that the modes are still symmetric with respect to the midplane. The structure of the instability is similar to the one obtained in [15] and the localization of the energy of the mode indeed suggests that the instabil-

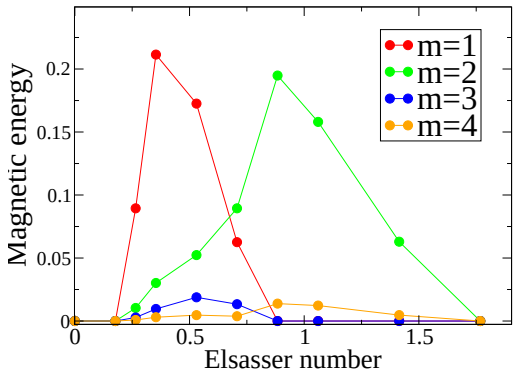


FIG. 4: Bifurcation diagram of the magnetic energy when the Elsasser number Λ is increased for a fixed Reynolds number $Re = 2000$. Note the non-axisymmetric destabilization of the meridional return flow by the applied field, dominated by $m = 1$ and $m = 2$ non-axisymmetric modes. Strong applied fields suppress these MHD instabilities.

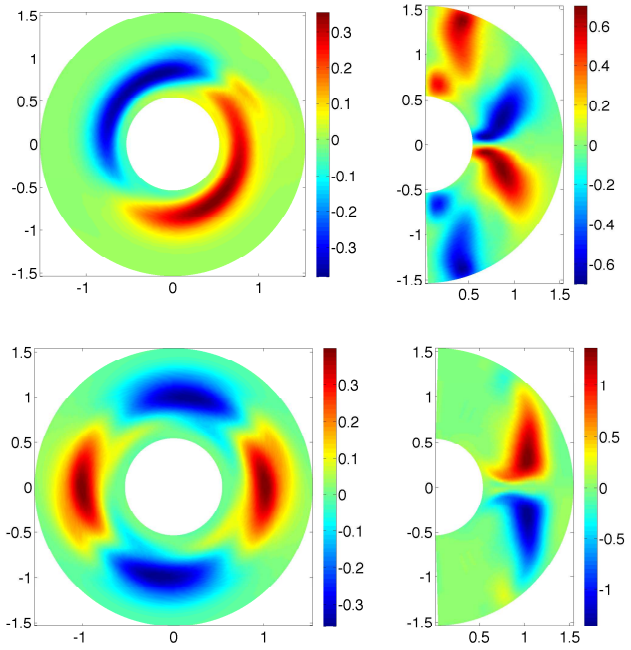


FIG. 5: Structure of the MHD instability for $Re = 2000$. The figure shows the radial non-axisymmetric component of the magnetic field just above the equatorial plane (left) or in a given meridional plane at $\phi = 0$(right). The two top figures show the $m = 1$ mode obtained for $\Lambda = 0.35$ and the two bottom figures show the field obtained for $\Lambda = 0.9$, dominated by the $m = 2$ azimuthal wavenumber.

ity is related to the meridional return flow. Note however that close to the threshold, our large Rm calculations lead to the generation of an $m = 1$ mode, whereas inductionless simulations of [15] predicted an $m = 2$ mode.

When $m = 1$ and $m = 2$ azimuthal modes are both excited, a phase locking is achieved between these two modes, and nonlinear interactions can become important. Finally, if the Elsasser number is increased up to 1.8, the magnetic tension of the applied magnetic field suppresses any instability, and the system comes back to an axisymmetric state.

III COMPARISON WITH MRI

At this point, we would like to briefly compare these instabilities, mainly due to the presence of boundaries, to what would be expected in a cylindrical geometry. Chandrasekhar [4] and Velikhov [2] first studied the effect of an axial applied magnetic field on a Couette flow confined between two infinite cylinders. They considered rotations of the cylinders such that the flow is stable under the centrifugal instability. According to the Rayleigh criterion, this means that the rotation profile follows $\Omega \sim r^\gamma$, with $\gamma > -2$. However, this flow can be destabilized by applying an magnetic field to the system if $\gamma < 0$. This powerful magnetorotational instability (MRI), later rediscovered by Balbus and Hawley in the framework of accretion disks, yields a radial outflow of angular momentum and can lead to an MHD turbulent state. The magnetic field can also have a stabilizing effect: for unstable flow satisfying $\gamma < -2$, the magnetic field is able to suppress the centrifugal instability [3]. Finally, the MRI is also suppressed if the applied magnetic field is too strong.

Despite the fact that MRI is generally considered as a local instability (without regard to the boundaries of the system) , it is interesting to note that most of the above features are encountered in the instabilities of our finite geometry system. First, figure 2 shows that the MHD instability is excited only in a delimited pocket in the parameter space: it requires a finite value of the magnetic field to be unstable, but is stabilized if the applied magnetic field is too strong. Second, the critical value of the Elsasser number for restabilization rapidly increases with Rm, similarly to the magnetorotational instability. In addition, one can find similarities between the suppression of the hydrodynamical instability by the magnetic field and the suppression of the centrifugal instability in Taylor-Couette flow.

From an astrophysical point of view, an important characteristic of the MRI is its ability to ensure an efficient outward transport of the angular momentum and to yields accretion, and eventually turbulence. Since there are different ways to measure the level of fluctuations in our simulations, we compare three differ-

ent quantities. For instance, we computed the quantity $\zeta = \frac{\sqrt{<(u_\phi - <u_\phi>)^2>}}{\sqrt{<u_\phi>^2}}$, measuring the level of fluctuation of u_ϕ, where $<>$ denotes time averaging. The velocity is probed in the equatorial plane at $r = 0.7$ and $\phi = 0$. Figure 6 shows the evolution of ζ when the Elsasser number is increased, for a fixed value of the Reynolds number $Re = 1000$. In figure 6, we also show the evolution of the parameter $\beta = \frac{<(u_\phi - <u_\phi>)(u_r - <u_r>)>}{<u_\phi>^2}$ related to the Reynolds stress, and the evolution of the excess torque G applied on the inner sphere, which quantify the amount of angular momentum transported. For this value of $Re = 8000$, the purely hydrodynamical state consists of a basic spherical Couette flow associated with an $m = 2$ component, and the total kinetic energy is steady. As Λ is increased, the flow becomes unstable to several azimuthal wavenumbers, and non-linear interactions rapidly lead to a chaotic evolution of the flow. As can be seen on figure 6, this corresponds to a growth of the three quantities ζ, β and G, evidencing an increase of the level of turbulence and of the amount of angular momentum transported outward. This transition is illustrated by the two snapshots of figure 6: for $\Lambda = 0$ (left), the radial flow taken at $r = (r_o + r_i)/2$ is dominated by a smooth $m = 2$ perturbation. For $\Lambda = 1$ however (right), far from the MHD instability onset, the velocity field appears more fluctuating and spatially disorganized. It is remarkable that the three different quantities used to measure this transition show a good agreement. This is particularly interesting for comparison between different experiments, where only either torque or velocity measurements are often available.

Here again, we find that this instability plays a role similar to the MRI, by destabilizing an otherwise stable flow and leading to a strong MHD turbulent state. These striking similarities between our instability and the magnetorotational instability have important consequences for experimental studies of the MRI. In particular, it points out the difficulties to make a clear distinction between both types of instability from experimental diagnostics. In the next section, we therefore compare our numerical simulations to experimental results obtained in the Maryland experiment, which have been interpreted as non-axisymmetric MRI.

IV COMPARISON WITH EXPERIMENTS: AXIAL FIELD AND OUTER SPHERE AT REST

In this section, we now keep the outer sphere at rest, and the applied magnetic field is purely axial, aligned with the axis of rotation. While the outer sphere is always taken insulating, two types of boundary conditions have been used for the inner sphere: insulating or conducting (with the same electrical conductivity as the fluid). This configuration is similar to the one used

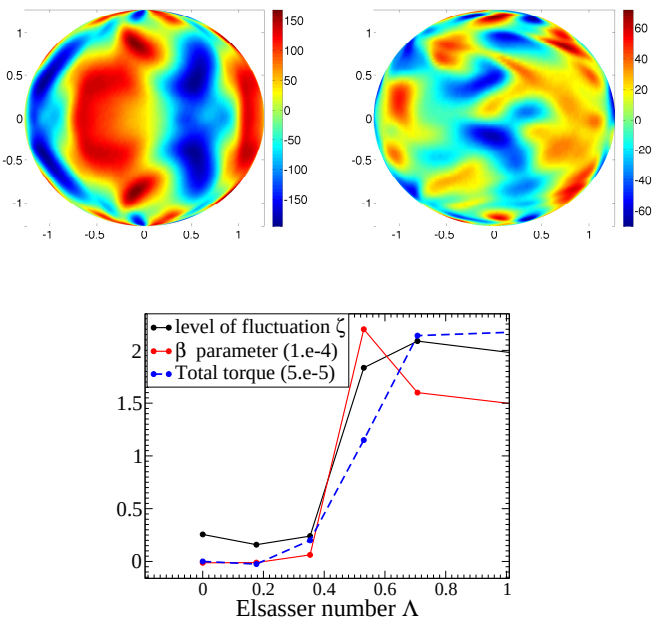


FIG. 6: Effect of the imposed magnetic field on the turbulence level, for $Re = 8000$ and $\Omega_i = 8\Omega_o$. Top: non-axisymmetric u_ϕ at the spherical surface of radius $r = 1.2$ showing that for $\Lambda = 0$. (left), the flow is dominated by an $m = 2$ mode due to an hydrodynamic instability, and is weakly fluctuating. Right: For $\Lambda = 1$, when boundary-driven instabilities are generated by the applied field, the flow becomes more complicated and chaotic. Bottom: evolution of the turbulence intensity when the magnetic field is increased. MHD instabilities due to boundaries yield turbulent fluctuations and angular momentum transport, similarly to the MRI.

in the Maryland experiment. This experiment consists of Sodium flowing between an inner sphere of radius $a = 0.050$ m and an outer sphere of radius $b = 0.15$ m. The inner sphere is made of high conductivity copper, and an external axial magnetic field is applied coaxially using a pair of electromagnets. In [8], the authors report that axisymmetric and non-axisymmetric modes are spontaneously excited for sufficiently large Rm when a magnetic field is applied. Most of the parameter space is dominated by an $m = 1$ precessing pattern, and the appearance of these instabilities is correlated with a strong increase of the torque applied on the inner sphere. Some of the non-axisymmetric modes are suppressed for large magnetic field. These results have been interpreted by the authors to be a signature of the magnetorotational instability. Note that since the outer sphere is at rest, the background flow is already very turbulent without applied field, in contrast with the initial stable laminar state generally considered in studies of MRI.

As can be seen in figure 7, the flow without magnetic field is very different from the one obtained in the pre-

vious sections, when the outer sphere was rotating: a strong equatorial jet is produced in the midplane, and no Stewartson layer is generated. It is useful to introduce the velocity exponent $\gamma = \partial \log \Omega(r)/\partial \log r$, where $\Omega(r)$ is the rotation rate at a cylindrical radius r. The Rayleigh criterion for stability, $\gamma > -2$, is thus expected to be violated when the outer sphere is at rest. However, in [8], a very weak level of turbulent fluctuations has been reported, together with a velocity exponent around -1.5, surprisingly close to a stable keplerian flow. In figure 7, we show the radial profile of $\gamma(r)$, for different altitudes z in a purely hydrodynamical simulation. Except near the boundaries (where the flow is strongly Rayleigh unstable), stable profiles with $\gamma > -2$ can be obtained, depending on the altitude z (for instance, $\gamma \sim -1$ at $z = 0.2$). However, as the measurements are done closer to the midplane, the velocity exponent significantly decreases, and unstable profiles are obtained, with γ much smaller than -2. This is also the case if z is too large. This variability of the angular profile underlines the difficulties of studying the MRI in a spherical Couette flow, particularly in the absence of global rotation uniformizing the flow in the axial direction.

As Re is increased, the flow undergoes bifurcations to non-axisymmetric modes. Indeed, it is well known that for sufficiently large Reynolds number, the equatorial jet becomes unstable to non-axisymmetric perturbations, and gives rise to a Kelvin-Helmoltz instability. The critical wavenumber for this instability depends on the aspect ratio and on the Reynolds number. Figure 8 shows a bifurcation diagram of the kinetic energy as Re is increased. The flow bifurcates to a non-axisymmetric state at $Re = 2700$, where the equatorial jet is destabilized to an $m = 3$ structure. For higher Re, there is a transition to an $m = 2$ mode. It is numerically expensive to conduct simulations at higher Reynolds numbers, but it is expected that successive bifurcations involving higher azimuthal wavenumbers eventually yield a turbulent state. It has been recently shown that these non-axisymmetric instabilities can trigger dynamo action, but only when $Pm > 1$ [25], which will not be considered here. An important feature is that these non-axisymmetric modes are antisymmetric, in contrast with the symmetric hydrodynamical modes obtained when the outer sphere is rotating.

Let us now study the magnetized regime. In this section, the magnetic Prandtl number is set to $Pm = 0.01$, which allows us to obtain magnetic Reynolds number Rm comparable to the ones used in the Maryland experiment. In the presence of an external axial magnetic field, the system exhibits most of the features obtained with a rotating outer sphere and described in the previous section of this article. For instance, when a magnetic field is applied to the hydrodynamical state, the non-axisymmetric destabilizations of the equatorial jet can be suppressed. Various non-axisymmetric states, different from this equatorial jet instability, are also generated by the magnetic field. In figure 7-right, we show the flow obtained when a strong axial magnetic field is applied (with a conducting inner sphere).

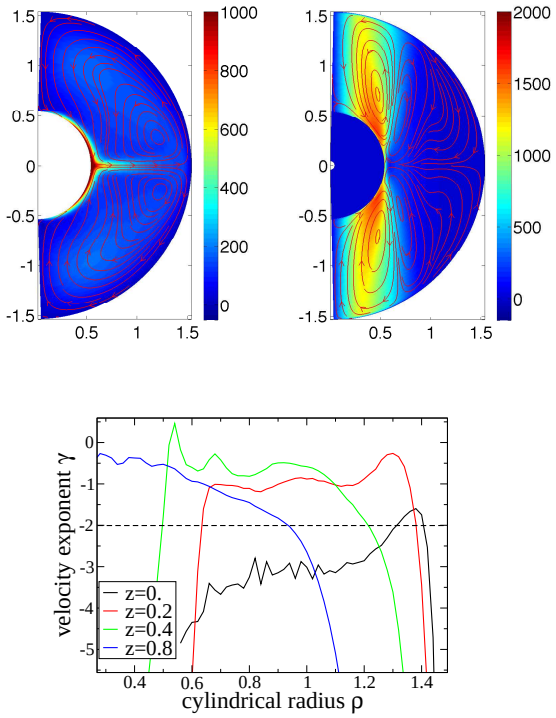


FIG. 7: Top: Structure of the spherical Couette flow when the outer sphere is now at rest, for $\Lambda = 0$ (left) and $\Lambda = 2$ (right), with $Re = 5000$. Colors indicate azimuthal flow u_ϕ and streamlines show the meridional recirculation. Note the absence of Stewartson layer in the purely hydrodynamical case (no global rotation) and the generation of the Shercliff layer in the magnetized one. Bottom: Velocity exponent γ taken at different altitude z, for $\Lambda = 0$. Note the Rayleigh unstable profiles ($\gamma < -2$) close to the midplane.

In this case, the particular surface Σ (which separates flow into two regions according to whether magnetic field lines are touching both spheres or only one of them) is located on the tangent cylinder: the fluid is at rest with the outer sphere outside the tangent cylinder, while the fluid inside the tangent cylinder rotates at Ω_i (for a conducting inner sphere) or at the intermediate rate $\Omega_i/2$ (for an insulating inner sphere). The spatial extension of the Ekman recirculation is also reduced. As noted before, this shear layer becomes unstable to non-axisymmetric perturbations for sufficiently large Reynolds number. For smaller values of the applied field, the return flow instability described in the previous section is also generated.

Figure 9 shows the evolution of the magnetic energy of

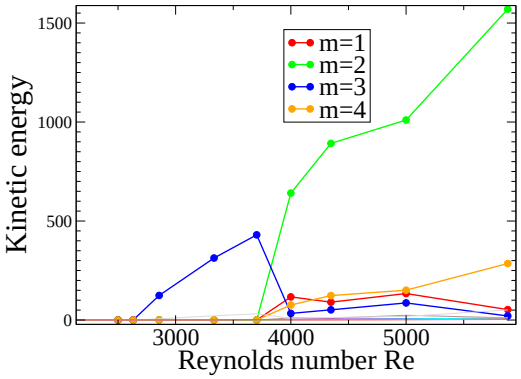


FIG. 8: Bifurcation diagram of the total kinetic energy when Re is increased. The outer sphere is at rest and Elsasser number is set to zero. As Re is increased, the equatorial jet adopts a wavy structure corresponding to non-axisymmetric modes, first $m = 3$ then $m = 2$. For larger Re, it is expected that the flow tends to a fully turbulent state.

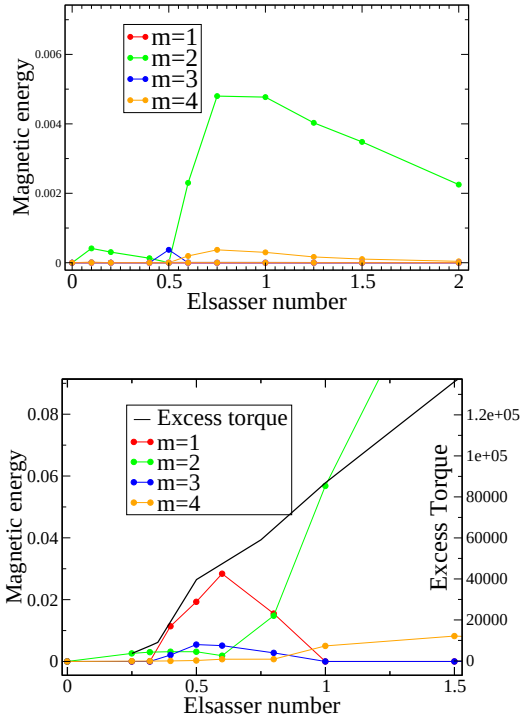


FIG. 9: Bifurcation diagram of the magnetic energy when Λ is increased, for $Re = 5000$ and $Rm = 50$, with an outer sphere at rest and an axial applied magnetic field (Maryland experiment configuration). Top: insulating inner sphere. Bottom: conducting inner sphere. In the latter case, a good agreement with the Maryland experiment is obtained, including the generation of an $m = 1$ mode and increase of the torque on the inner sphere (to be compared with Fig.4 of [8]).

different azimuthal modes for $Re = 5000$ and $Rm = 50$ as a function of the Elsasser number Λ.

In figure 9-top, the inner sphere is insulating. In the whole range of Elsasser numbers explored here, the magnetic energy is dominated by an $m = 2$ instability. At small Elsasser number ($\Lambda < 0.5$), this corresponds to the hydrodynamical jet instability, equatorially antisymmetric, which extends into the magnetized regime. For $\Lambda > 0.5$, a different instability occurs, which is symmetric with respect to the equator. Figure 10 shows the structure of this instability for two different Elsasser numbers. As Λ is increased, the oscillations gradually transits from a return flow instability associated with the meridional recirculation (top, $\Lambda = 0.6$), to a Shercliff layer instability (bottom, $\Lambda = 2$). In the latter case, the energy is concentrated on the tangent cylinder and consists of a series of vortices roughly independent of the z-direction.

In figure 9-bottom, the inner sphere is electrically conducting. The electrical conductivity is identical to that of the fluid, and thus smaller than the conductivity used in the Maryland experiment, where an inner sphere made of copper is used. In spite of this difference and of our lower Reynolds number, our numerical simulations show a very good agreement with the results obtained in the experiment (see for instance figure 4 of [8]):

- An $m = 1$ mode is generated in a range of the Elsasser number similar to the experiment. The generation of this $m = 1$ mode is clearly due to the conductivity of the inner sphere. Note in particular that this instability is antisymmetric with respect to the equator, unlike Shercliff or return flow instabilities. However, the instability is still concentrated near the tangent cylinder(see figure 11).

- This non-axisymmetric mode can be suppressed by a strong field, and a transition between different azimuthal wavenumbers is observed for higher fields, in agreement with the Maryland experiment.

- The structure of the radial magnetic field, as shown in figure 11, possesses the same symmetry with respect to the equator as the first mode obtained in the Maryland experiment. At larger Elsasser number, this $m = 1$ instability is replaced by return flow instability and Shercliff layer instability, rather equatorially symmetric. This change of symmetry has also been reported in the Maryland experiment.

-The suppression of the $m = 1$ mode and the generation of a smaller $m = 2$ mode when the inner sphere is switched from conducting to insulating has also been

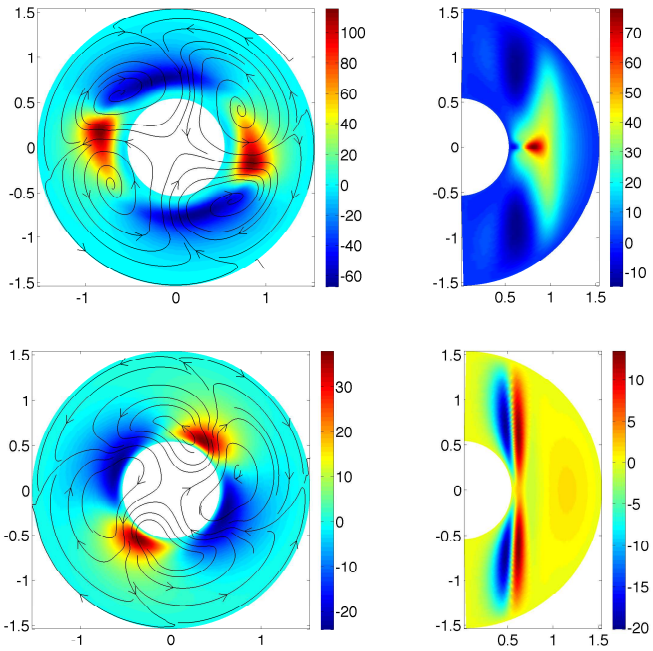


FIG. 10: Structure of the MHD instabilities for $Re = 5000$ with an insulating inner sphere and an axial field, formed of vortices in the horizontal plane. Figure shows the radial non-axisymmetric component of the velocity field u_r in the equatorial plane (left) or in a given meridional plane at $\phi = 0$(right). The two top snapshots show the $m = 2$ mode obtained for $\Lambda = 0.6$ (instability related to the meridional return flow) and the two bottom snapshots show the field obtained for $\Lambda = 2$. (Shercliff layer instability).

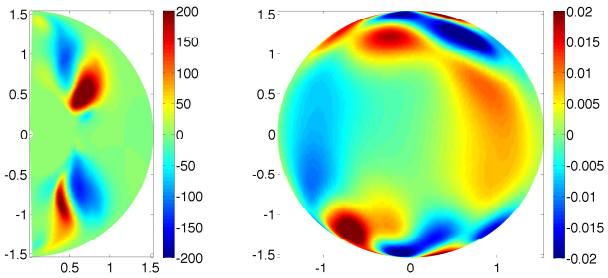


FIG. 11: Structure of the $m = 1$ instability obtained for $\Lambda = 0.5$, $Re = 5000$ and $Rm = 50$, in the case of a conducting inner sphere. Left: non-axisymmetric V_r in the meridional plane at $\phi = 0$. Right: non-axisymmetric B_r at the surface of the outer sphere. The structure is identical to the mode observed in the Maryland experiment, with the same equatorial and azimuthal symmetries.

observed in the Maryland experiment [26].

- Finally, we computed the evolution of the excess torque applied to the inner sphere in the conducting case. Like in the previous section, as the flow becomes unstable to non-axisymmetric perturbations, we observe a strong increase of the total torque applied to the inner sphere (see the black curve in figure 9-bottom). This evolution has been interpreted as an indication of MRI in the Maryland experiment. The fact that our simulations reproduce this feature suggests that Shercliff layer and return flow instabilities are also efficient mechanisms to enhance the amount of angular momentum transported outward. However, a large amount of the augmentation of our torque for this conducting case and the one reported in the Maryland experiment could be simply due to the attachment of magnetic field lines to the inner conducting sphere. Indeed, analytical calculations of a rotating conducting sphere with a uniform axial imposed field and surrounded by an infinite medium of stationary Sodium, predict an important rise of the torque [27]. Applied to our configuration, these calculations lead to a torque of the same order of magnitude than the one reported in the figure 9. In any case, this shows that the torque measured in the Maryland experiment cannot be assumed to be a direct reflection of MRI instabilities.

An important observation is that both Shercliff layer instability and return flow instability are inductionless instabilities, in the sense that they can be generated for arbitrary small magnetic Reynolds number if the hydrodynamical Reynolds number is large enough. Figure 12 shows for instance the $m = 2$ instability obtained for $Re = 5000$, $Rm = 0.5$, $\Lambda = 1.5$ and a conducting inner sphere. Note that this $m = 2$ mode is in good agreement with inductionless calculations of [15], in which a similar setup is used (except for the magnetic boundary condition on the inner sphere which is insulating in [15]). This underlines the difference of nature between the boundary driven instability reported here and the standard MRI (for which induction is necessary), despite the strong similarities between both instabilities.

The several similarities between our simulations and the results of the Maryland experiment emphasize the importance of considering the role of boundaries in MRI experiment. These numerical simulations indeed strongly suggest that the non-axisymmetric modes observed in the experiment are destabilizations of either the Shercliff layer (at large applied field) or the return flow (at smaller applied field), rather than the MRI. These instabilities appear to be very robust, and extend in a large region of the parameter space. This is therefore reasonable to expect them to occur in the Maryland experiment, which uses a setup similar to our numerical problem.

In addition to these non-axisymmetric modes, an $m = 0$ mode equatorially symmetric has also been reported

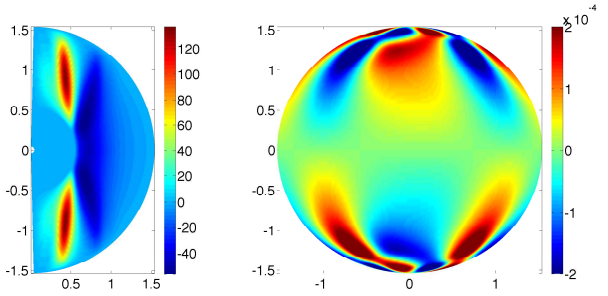


FIG. 12: Structure of the non-axisymmetric component of the Shercliff layer instability for $Re = 5000$, $Rm = 0.5$ and $\Lambda = 1.5$, with a conducting inner sphere. Left: non-axisymmetric u_r in the meridional plane $\phi = 0$. Right: non-axisymmetric B_r at the surface of the outer sphere. Induction is not a necessary condition for the instability to be generated.

in the Maryland experiment. It is interesting to mention that this axisymmetric mode measured in the experiment has not been obtained in our numerical simulation at $Pm < 1$. However, for $Pm \sim 1$, axisymmetric modes are generated in the simulations with an axial magnetic field, with or without global rotation. They seem analogous to magnetostrophic MRI modes, a modified version of the MRI in spherical geometry, possibly relevant to the Earth core [28] but relying on a magnetostrophic equilibrium not achieved in our simulations. Their analysis is beyond the scope of this paper, and will be studied in a future work. This $m = 0$ mode thus could be of a different nature than the non-axisymmetric ones, and may not be related to the Shercliff layer.

CONCLUSION

In this article, the flow of an electrically conducting fluid in a spherical shell has been studied numerically. When a magnetic field is applied to the system, two different effects are observed. First, non-axisymmetric hydrodynamical bifurcations from the Stewartson layer or from the equatorial jet can be suppressed by a sufficiently strong magnetic field. But the applied field also has a destabilizing effect, by either disrupting the axisymmetry of the meridional return flow, or through a two-step process: first, an axial or dipolar applied field creates a Shercliff layer, and second, this MHD shear layer eventually becomes unstable to non-axisymmetric modes if the magnetic field is not too strong.

We have seen that this Shercliff layer instability, or the meridional return flow instability, are dominated by different azimuthal wavenumbers depending on the parameters (Re, Λ) and the details of the configuration. These instabilities are very important in the context of laboratory studies of the magnetorotational instability. Indeed, they are relatively robust, and share a lot of characteristics with the non-axisymmetric MRI. The marginal stability curve is similar, with a destabilization occurring only in a given range of the value of the applied field. Whereas a finite value of the field is required to trigger the instability, the free energy come from the azimuthal velocity and its associated differential rotation (at least in the case of the Shercliff layer instability). Moreover, we have shown that, like the MRI, these instabilities yield an MHD turbulent state, and are very efficient to transport the angular momentum outward. It is however important to insist on the fact that Shercliff layer and return flow instabilities are inductionless (unlike the standard MRI), and rely on a different destabilization mechanism.

These similarities have important consequences for laboratory studies of the MRI. First, as was suggested in [15], our numerical simulations strongly confirm that results of the Maryland experiment are related to these boundary driven instabilities rather than MRI. A very good agreement is obtained with experimental observations, including the sequence of non-axisymmetric bifurcations, the geometry of the magnetic field and the increase of the torque on the inner sphere. This work could also have interesting echos for investigation of the MRI in a cylindrical geometry. In this case, the finite geometry imposed by the experimental approach makes it impossible to obtain an ideal Couette flow or a quasi-Keplerian flow, because of the poloidal recirculation created by the viscous stress at the vertical endcaps. This problem has been circumvented by replacing the rigid endcaps at the top and the bottom by two rings that are driven independently. It has been shown that a flow profile in a short Taylor-Couette cell can be kept stable until $Re \sim 10^6$ if the appropriate configuration of split end caps is used [5]. Similarly, the use of such split rings in the Promise experiment has led to a significant reduction of the Ekman pumping and a much clearer identification of the HMRI [29]. Recent three-dimensional numerical simulations [30] suggest that the jump of angular velocity between inner and outer rings can be reinforced by applying an axial magnetic field, and extended in the z direction. This leads to the creation of a Shercliff layer very similar to the one described in this paper, which also undergoes some transition to non-axisymmetric modes. It is thus possible that similar instabilities could be generated from the Shercliff layer or from the poloidal return flow in these cylindrical MRI experiments. This interpretation is reinforced by the fact that the modes observed in the Princeton MRI experiment appear to be inductionless [31].

Finally, our numerical simulations show that investigation of the MRI in the laboratory is significantly complicated by the presence of no-slip boundaries. In spherical or cylindrical geometry, the applied magnetic field interacts with these boundaries and can trigger MHD instabilities very similar to the MRI. It could make very difficult any distinction between these instabilities and

MRI in an experiment. The inductionless nature of Shercliff layer instability, in contrast to the required induction for standard MRI, may be an important key for the needed distinction between them. However, as pointed in the introduction, standard MRI continuously connects to the Helical MRI (HMRI) [32], an inductionless version of the MRI which can be regarded as an inertial oscillation destabilized by resistive MHD in presence of an helical magnetic field [33]. In this particular case, it would be interesting to see how our boundary-driven instabilities can therefore be related to global manifestations of the MRI.

This work was supported by the NSF under grant AST-0607472, by the NASA under grant numbers ATP06-35 and APRA08-0066, by the DOE under Contract No. DE-AC02-09CH11466, and by the NSF Center for Magnetic Self-Organization under grant PHY-0821899. We have benefited from useful discussions with E. Edlund, A. Roach, E. Spence and R. Hollerbach.

[1] Balbus, S. A. and Hawley, J. F., Astroph. Journ., **376**,314-233 (1991)
[2] E. P. Velikhov, J. Sov. Phys. JETP **36**, 995 (1959)
[3] S. Chandrasekhar, Hydrodynamic and hydromagnetic stability, (1961)
[4] Chandrasekhar S., (1960), Proc. Natl. Acad. Sci., 46, 253
[5] H. Ji, M. Burin, E. Schartman and J. Goodman, Nature **444**, 343 (2006).
[6] M. Nornberg, H. Ji, E. Schartman, A. Roach, and J. Goodman, Phys. Rev. Lett. **104**, 074501 (2010).
[7] F. Stefani et al, Phys. Rev. Lett. **97**, 184502 (2006)
[8] D. Sisan et al, Phys. Rev. Lett. **93**, 114502 (2004)
[9] R. Hollerbach, Proc Roy Soc A, 444, 333-346 (1994)
[10] Kleeorin, N., Rogachevskii, I., Ruzmaikin, A., Soward, A. M., Starchenko, S., J. Fluid Mech. 344, 213-244. (1997)
[11] S. V. Starchenko, Phys. of Fluids, **10**, 2412-2420 (1998)
[12] E. Dormy, P. Cardin, D. Jault, Earth and Plan. Sci. Lett., **160**, 15-30, (1998)
[13] D. Brito, T. Alboussiere, P. Cardin, N. Gagniere, D. Jault, P. La Rizza, J.P. Masson, H.C. Nataf, D. Schmitt, arXiv:1102.5173v1 [physics.geo-ph] (2011)
[14] H.-C. Nataf, T. Alboussiere, D. Brito, P. Cardin, N. Gagniere, D. Jault, D. Schmitt, Physics Earth Planet Inter, 170, 60-72 (2008)
[15] R. Hollerbach, Proc. R. Soc., **465**, 2003-2013 (2009)
[16] V. Travnikov, K. Eckert and S. Odenbach, Acta Mechanica 2011, DOI: 10.1007/s00707-011-0452-8
[17] R. Hollerbach and S. Skinner, Proc. R. Soc. Lond., **457**, 785-802 (2001)
[18] X.Wei and R. Hollerbach, Phys. Rev. E **78**, 026309 (2008)
[19] Christensen et al, Phys. Earth Planet. Int, **128**, 25-34 (2001)
[20] I. Proudman, J. Fluid Mech.,1:5:505-516 (1956)
[21] K. Stewartson, J. Fluid Mech., **26**, 131-144 (1966)
[22] A. Kageyama, H. Ji and J. Goodman, J. Phys Soc. Japan, **73**, 2424 (2004)
[23] J. A. Shercliff, Mat. Proc. of the Camb. Phil. Soc., **49**, 136-144 (1953)
[24] R. Hollerbach, E. Canet, A. Fournier, Euro. Journ. of Mech. B/Fluids **26** 729-737 (2007)
[25] C. Guervilly and P. Cardin (2010) Geophys. Astrophys. Fluid Dynamics, 104, 221-248
[26] D.R. Sisan, Ph.D. Thesis (2004)
[27] Jeremy Goodman, private communication.
[28] Petitdemange, L., Dormy, E., and Balbus, SA (2008), Geophys. Res. Lett. 35, L15305
[29] Stefani et al, Phys. Rev. E 80, 066303 (2009)
[30] Gissinger et al, in preparation (2011)
[31] A. Roach, E. Spence, E. Edlund, P. Sloboda and H. Ji, Bull. Am. Phys. Soc., **55**: BAPS. (2010)
[32] Hollerbach et al., PRL 95, 124501 (2005)
[33] Kirillov et al., ApJ 712, 52-68, (2010)